^{68}Ga-DOTA-FAPI-04 PET/MR in the Evaluation of Gastric Carcinomas: Comparison with ^{18}F-FDG PET/CT

Chunxia Qin*[1,2], Fuqiang Shao*[1,2], Yongkang Gai[1,2], Qingyao Liu[1,2], Weiwei Ruan[1,2], Fang Liu[1,2], Fan Hu[1,2], and Xiaoli Lan[1,2]

[1]*Department of Nuclear Medicine, Union Hospital, Tongji Medical College, Huazhong University of Science and Technology, Wuhan, China; and* [2]*Hubei Key Laboratory of Molecular Imaging, Union Hospital, Tongji Medical College, Huazhong University of Science and Technology, Wuhan, China*

We sought to evaluate the performance of ^{68}Ga-DOTA-FAPI-04 (^{68}Ga-FAPI) PET/MR for the diagnosis of primary tumor and metastatic lesions in patients with gastric carcinomas and to compare the results with those of ^{18}F-FDG PET/CT. **Methods:** Twenty patients with histologically proven gastric carcinomas were recruited, and each patient underwent both ^{18}F-FDG PET/CT and ^{68}Ga-FAPI PET/MR. A visual scoring system was established to compare the detectability of primary tumors and metastases in different organs or regions (the peritoneum, abdominal lymph nodes, supradiaphragmatic lymph nodes, liver, ovary, bone, and other tissues). The original SUV_{max} and normalized SUV_{max} (calculated by dividing a lesion's original SUV_{max} with the SUV_{mean} of the descending aorta) of selected lesions on both ^{18}F-FDG PET/CT and ^{68}Ga-FAPI PET/MR were measured. Original/normalized $SUV_{max\text{-}FAPI}$ and $SUV_{max\text{-}FDG}$ were compared for patient-based (including a single lesion with the highest activity uptake in each organ/region) and lesion-based (including all lesions [≤5] or the 5 lesions with highest activity [>5]) analyses, respectively. **Results:** The 20 recruited patients (median age: 56.0 y; range: 29–70 y) included 9 men and 11 women, 14 patients for initial staging and 6 for recurrence detection. ^{68}Ga-FAPI PET was superior to ^{18}F-FDG PET for primary tumor detection (100.00% [14/14] vs. 71.43% [10/14]; $P = 0.034$), and the former had higher tracer uptake levels ($P < 0.05$). ^{68}Ga-FAPI PET was superior to ^{18}F-FDG PET in both patient-based and lesion-based evaluation except for the metastatic lesions in supradiaphragmatic lymph nodes and ovaries. Additionally, multiple sequences of MR images were beneficial for the interpretation of hepatic metastases in 3 patients, uterine and rectal metastases in 1 patient, ovarian lesions in 7 patients, and osseous metastases in 2 patients. **Conclusion:** ^{68}Ga-FAPI PET/MR outperformed ^{18}F-FDG PET/CT in visualizing the primary and most metastatic lesions of gastric cancer and might be a promising method, with the potential of replacing ^{18}F-FDG PET/CT.

Key Words: fibroblast activation protein; ^{68}Ga-FAPI; PET/MR; gastric cancer; ^{18}F-FDG

J Nucl Med 2022; 63:81–88
DOI: 10.2967/jnumed.120.258467

Gastric cancer is the fifth most common malignant tumor and the third most common cause of cancer death in the world (*1*). It has typical characteristics of high incidence, high metastasis rate, high mortality rate, low early diagnosis rate, low radical resection rate, and low 5-y survival rate (*2*). Many gastric cancer patients present with advanced-stage disease because of the lack of specific early signs and symptoms. Early diagnosis and accurate staging are crucial for choosing an appropriate therapy strategy (*3*).

^{18}F-FDG PET/CT is extensively used in the diagnosis, staging, and preoperative evaluation of gastric cancer. However, ^{18}F-FDG PET/CT has been reported to have a low detection rate for primary gastric cancer (~55%), especially in the early stage, as well as signet-ring cell, mucinous, and poorly differentiated adenocarcinomas, which are typically less metabolically active (*4*). Moreover, variable and occasionally intense physiologic uptake exist within the gastric wall, which can cover ^{18}F-FDG uptake by the primary tumor, and the presence of gastritis may cause false-positive results (*5*). In addition, Stahl et al. showed that the intensity of tumor ^{18}F-FDG uptake is not predictive of survival (*6*). Therefore, other more sensitive PET probes are needed for the diagnosis and staging of gastric cancer.

Fibroblast activation protein (FAP) is overexpressed in cancer-associated fibroblasts of several tumor entities (*7*). FAP inhibitors (FAPIs) can specifically target and bind to FAP. FAPIs have been radiolabeled and used as probes to visualize FAP-expressing tumors. The probes including ^{68}Ga-FAPIs have demonstrated promising results in various cancers, including lung cancer, breast cancer, prostate cancer, sarcoma, and head and neck cancer (*8*,*9*). Different from ^{18}F-FDG PET, which reflects the glucose metabolism of tumor cells, radiolabeled FAPI imaging may show the cancer-associated fibroblasts and extracellular fibrosis in tumor stroma. Recent studies indicated that primary tumors and most sites of metastases in patients with different cancers are well visualized using ^{68}Ga-FAPI PET/CT (*10*,*11*). However, the effect of FAPI imaging in gastric cancer has been described in only a few case reports (*12*,*13*) or in comprehensive studies involving many malignancies (*10*,*11*). Additionally, as previous research on FAPI mainly focused on PET/CT, the performance of PET/MR with FAPI needs to be clarified. In this study, we aimed to further evaluate the performance of ^{68}Ga-DOTA-FAPI-04 (abbreviated as ^{68}Ga-FAPI) PET/MR in gastric cancer and to compare it with that of ^{18}F-FDG PET/CT.

MATERIALS AND METHODS

Patients

This prospective study was approved by the institutional review board of Union Hospital, Tongji Medical College, Huazhong University of Science and Technology (IRB 20200290), and all subjects

Received Oct. 13, 2020; revision accepted Apr. 6, 2021.
For correspondence or reprints, contact Xiaoli Lan (xiaoli_lan@hust.edu.cn).
*Contributed equally to this work.
Published online Apr. 16, 2021.

TABLE 1
Clinical Characteristics of Patients with Gastric Cancer

No.	Sex	Age (y)	Role of PET	Pathology	Primary tumor	Confirmed metastases*	Clinical stage/ final diagnosis
1	Female	38	IS	PDAC	Whole stomach	PM, LNM, OM	IV
2	Female	36	IS	SRCC	Greater curvature of gastric body	PM, LNM, OM	IV
3	Male	66	IS	Nonkeratinizing squamous cell carcinoma	Esophagus-stomach cardia	LNM, LM, BM	IV
4	Male	56	IS	Adenocarcinoma	Gastric body	LNM, LM	IV
5	Male	58	IS	PDAC, partial SRCC	Gastric antrum, angular notch	LNM	IIIA
6	Female	70	IS	PDAC, partial SRCC	Whole stomach	PM, LNM	IV
7	Male	61	IS	Moderately differentiated adenocarcinoma	Whole stomach	LNM, LM, abdominal wall†	IV
8	Male	61	IS	Low-adhesion Carcinoma, partial SRCC	Stomach pylorus	PM, LNM	IV
9	Female	59	IS	PDAC	Gastric antrum, angular notch	LNM, BM	IV
10	Male	66	IS	PDAC	Greater curvature of gastric body	PM, LNM, BM	IV
11	Male	58	IS	SRCC	Angular notch	LNM	IV
12	Female	35	IS	PDAC, partial SRCC	Gastric body	LNM	IIIB
13	Male	50	IS	SRCC	Stomach pylorus-duodenal bulb	None	II
14	Male	63	IS	Adenocarcinoma	Remnant stomach	PM, LNM	IV
15	Female	54	RD	PDAC		PM, OM	PD
16	Female	33	RD	Low-adhesion carcinoma		PM, LNM, OM, left ureter†	PD
17	Female	29	RD	PDAC		PM, OM	PD
18	Female	50	RD	PDAC		PM, OM	PD
19	Female	56	RD	SRCC		LNM	PD
20	Female	45	RD	PDAC, partial SRCC		LN, uterus†, rectum†	PD

*Metastases were confirmed by the comprehensive consideration of imaging findings and pathologic results.
†Metastases at uncommon sites.
IS = initial staging; PDAC = poorly differentiated adenocarcinoma; PM = peritoneal metastasis; LNM = lymph node metastasis; OM = ovarian metastasis; SRCC = Signet ring cell carcinoma; LM = liver metastasis; BM = bone metastasis; RD = recurrence detection; PD = progression of disease.

signed a written informed consent form. Twenty patients with gastric cancer were enrolled from June 2020 to July 2020. The key eligibility criteria were as follows: having histologically proven gastric carcinomas for initial staging or recurrence detection after therapy, having no prior treatment within 4 wk before PET imaging, having no contraindications to MRI, agreeing to undergo both ^{18}F-FDG PET/CT and ^{68}Ga-FAPI PET/MR, and undergoing 2 scans with an interval of less than 1 wk.

^{18}F-FDG PET/CT

^{18}F-FDG was synthesized with ^{18}F produced by a cyclotron (MINItrace; GE Healthcare), with a radiochemical purity of more than 95%. ^{18}F-FDG (3.70–5.55 MBq/kg) was administrated after the patient fasted for at least 6 h and had a normal blood glucose level. Imaging was performed approximately 60 min after administration using an integrated PET/CT scanner (Discovery VCT; GE Healthcare) from the top of the head to the upper thighs with the following parameters: 120 kV, 110 mAs, thickness of 3.75 mm. PET was acquired with 3 min per bed position.

^{68}Ga-FAPI PET/MR

^{68}Ga-FAPI was radiolabeled according to a previously described method (*11*). Briefly, ^{68}GaCl3 eluted from ^{68}Ge/^{68}Ga generator (ITG) was reacted with 20 μg (20 nmol) of FAPI-04 ligand (C S Bio Co.)

TABLE 2
Comparison of Semiquantitative Parameters Between ^{68}Ga-FAPI PET and ^{18}F-FDG PET

Parameter	Imaging modality	Primary tumor	Peritoneal metastases	Lymph node (abdominal)	Ovaries	Liver metastases	Bone metastases	Lymph node (supradiaphragm)
Patient-based analysis		14	10	12	7	3	3	7*
Patient number	^{18}F-FDG PET/CT	10	4	10	7	3	3	6
	^{68}Ga-FAPI PET/MR	14	10	12	7	3	3	6
	P	0.034	0.011	1	—	—	—	—
Original SUV_{max}	^{18}F-FDG PET/CT	6.18 ± 2.46	7.60 ± 5.85	6.58 ± 2.78	4.19 ± 1.72	5.63 ± 1.96	5.8 ± 5.39	8.42 ± 6.14
	^{68}Ga-FAPI PET/MR	11.31 ± 3.96	8.43 ± 3.46	9.93 ± 5.58	4.63 ± 2.17	6.30 ± 2.61	12.33 ± 5.70	6.93 ± 5.60
	P	0.002	0.743	0.086	0.680	0.741	0.223	0.671
Normalized SUV_{max}	^{18}F-FDG PET/CT	3.99 ± 1.53	4.97 ± 2.43	4.04 ± 1.76	3.00 ± 1.35	3.45 ± 0.48	3.16 ± 2.77	5.07 ± 2.78
	^{68}Ga-FAPI PET/MR	12.40 ± 5.17	9.58 ± 4.26	10.90 ± 6.17	4.88 ± 2.06	6.54 ± 1.67	11.76 ± 4.71	7.70 ± 4.80
	P	0.000	0.068	0.003	0.067	0.037	0.053	0.273
Lesion-based analysis								
Lesion number	^{18}F-FDG PET/CT		14	33	12	6	4	24
	^{68}Ga-FAPI PET/MR		42	45	12	13	12	18
	P		0.000	0.000	—	0.011	0.001	0.022
Original SUV_{max}	^{18}F-FDG PET/CT		5.74 ± 3.28	6.13 ± 2.79	3.74 ± 1.53	5.72 ± 1.33	5.2 ± 4.56	6.77 ± 4.83
	^{68}Ga-FAPI PET/MR		7.61 ± 2.98	8.65 ± 4.38	4.19 ± 1.76	5.81 ± 2.03	10.05 ± 6.18	6.41 ± 4.51
	P		0.052	0.003	0.511	0.915	0.167	0.807
Normalized SUV_{max}	^{18}F-FDG PET/CT		3.71 ± 1.53	3.73 ± 1.66	2.73 ± 1.08	3.30 ± 0.40	2.90 ± 2.32	3.96 ± 1.93
	^{68}Ga-FAPI PET/MR		8.74 ± 3.82	9.43 ± 5.01	4.38 ± 1.81	5.84 ± 1.44	9.48 ± 5.42	7.41 ± 4.06
	P		0.000	0.000	0.013	0.000	0.004	0.003

*Among the 7 patients with supradiaphragmatic lymph nodes, 5 patients were positive on both ^{68}Ga-FAPI and ^{18}F-FDG PET scans, and the remaining 2 patients were ^{68}Ga-FAPI–positive/^{18}F-FDG–negative and ^{68}Ga-FAPI–negative/^{18}F-FDG–positive, respectively.

— = No need to compare.

FIGURE 1. Representative images of ^{68}Ga-FAPI PET (A) and ^{18}F-FDG PET (B) in patients with gastric cancer for initial staging (patients 1, 2, 3, and 10) and recurrence detection (patients 18 and 19) (from left to right). ^{68}Ga-FAPI images are superior to ^{18}F-FDG images in visualization of primary tumors and metastases. ^{68}Ga-FAPI total scores were 8, 7, 6, 5, 3, and 2, respectively, and all of the ^{18}F-FDG total scores were 0.

using a manual synthesis module (ITG) in 1 mL of 0.25 M sodium acetate buffer for 5 min at 100°C and purified before use.

Imaging was performed approximately 30–60 min after the intravenous administration of ^{68}Ga-FAPI (a dose of 1.85–3.7 MBq/kg) using an integrated PET/MR scanner (SIGNA PET/MR; GE Healthcare). MR images (a high-resolution axial T1-weighted liver acquisition with volume acceleration-Flex sequence and a coronal T2-weighted fast recovery fast spin echo) from brain to upper thigh were acquired during the PET scan (3 min/bed position). Next, dedicated multiple-sequence MR images (T1- and T2-weighted images) and diffusion-weighted images (DWI) of the abdominal and pelvic cavity were acquired. All PET data were reconstructed using time-of-flight information with 3-dimensional ordered-subset expectation maximization protocol iterative reconstruction algorithms.

Image Interpretation

All images were registered on the AW workstation (version 4.6; GE Healthcare). To avoid bias, 2 groups of experienced nuclear medicine physicians independently analyzed the ^{18}F-FDG PET/CT and ^{68}Ga-FAPI PET/MR images. Image interpretation included visual analysis and quantitative assessment, and the results were discussed to reach a consensus.

Visual Analysis. Abnormally elevated ^{18}F-FDG/^{68}Ga-FAPI uptake, accompanied by the abnormal density/signal in the corresponding sites on CT/MRI, was interpreted as positive if the possibility of physiologic uptake, trauma, infection, and inflammation could be excluded. According to the location, lesions were divided into primary tumor and extragastric organs/regions, including the peritoneum, abdominal lymph nodes, liver, ovary, supradiaphragmatic lymph nodes, bone, and other tissues. Additionally, those lesions that were missed or insufficient for diagnosis using ^{18}F-FDG PET/CT and ^{68}Ga-FAPI PET and for which MR provided additional value for the interpretation, were also recorded.

A visual scoring system was established to compare the lesion detection capabilities of ^{18}F-FDG PET and ^{68}Ga-FAPI PET, based on the lesion area (primary tumor and peritoneal metastases) or number (positive lymph nodes, liver, bone, and other tissues metastases) or the obviousness (ovaries) detected in the same patient by the 2 imaging studies. If the area/number/obviousness of lesions detected by ^{68}Ga-FAPI PET was >1 and <3, 3–5 or >5 times more than that of ^{18}F-FDG PET, ^{68}Ga-FAPI PET was scored 1, 2, and 3, respectively, and vice versa. If the area/number of lesions detected by the 2 imaging modalities was the same, the score was 0.

Quantitative Assessment. Quantitative assessment mainly involved the comparison of ^{18}F-FDG and ^{68}Ga-FAPI uptake in the same lesion. Regions of interest were drawn around foci with increased uptake in the transaxial slices, and an original SUV_{max} was automatically obtained. To ensure that SUV_{max} was relatively comparable, the original SUV_{max} was normalized by the following formula:

$$\textit{Normalized SUVmax} = \textit{Original SUVmax}/\textit{SUVbkgd}. \quad \text{Eq. 1}$$

SUV_{bkgd} refers to average SUV of the descending aorta.

Quantitative assessment was also divided into patient-based and lesion-based investigations. The former included the primary tumor or a single lesion with the highest uptake in each organ/region, whereas the latter referred to the analysis including all lesions (≤5) or the 5 lesions with highest activity (>5) if multiple metastases exist.

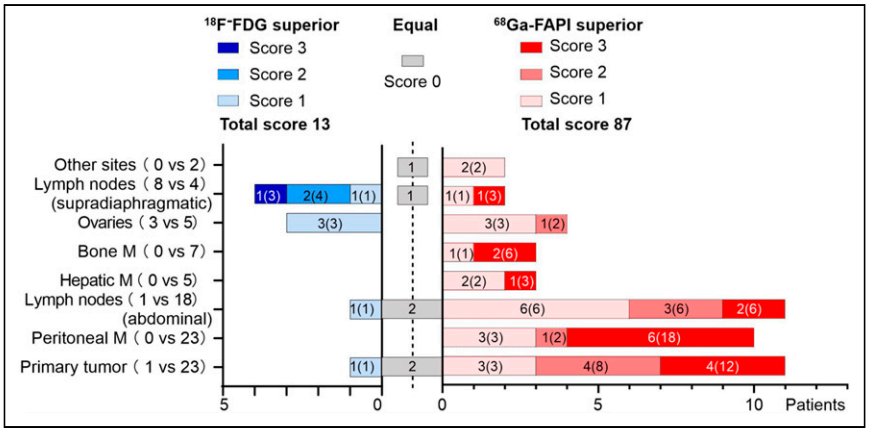

FIGURE 2. Comparison of visual assessment between ^{68}Ga-FAPI PET and ^{18}F-FDG PET. n(n) in each bar refers to patient number (scores); M = metastases.

Statistical Analysis

Statistical analysis was performed using SPSS software (version 22.0; IBM Inc.). Continuous variables are expressed as mean ± SD. Categoric variables are expressed as number and percentage. The number of positive lesions was compared using the χ^2 test, and the Student's t test was used to assess the differences of SUV_{max} between the 2 groups. A P value of less than 0.05 was defined as statistically significant.

RESULTS

Patient Characteristics

The median age of the cohort (9 men and 11 women) was 56.0 y (range: 29–70 y). The imaging studies were performed in 14 patients for initial staging and

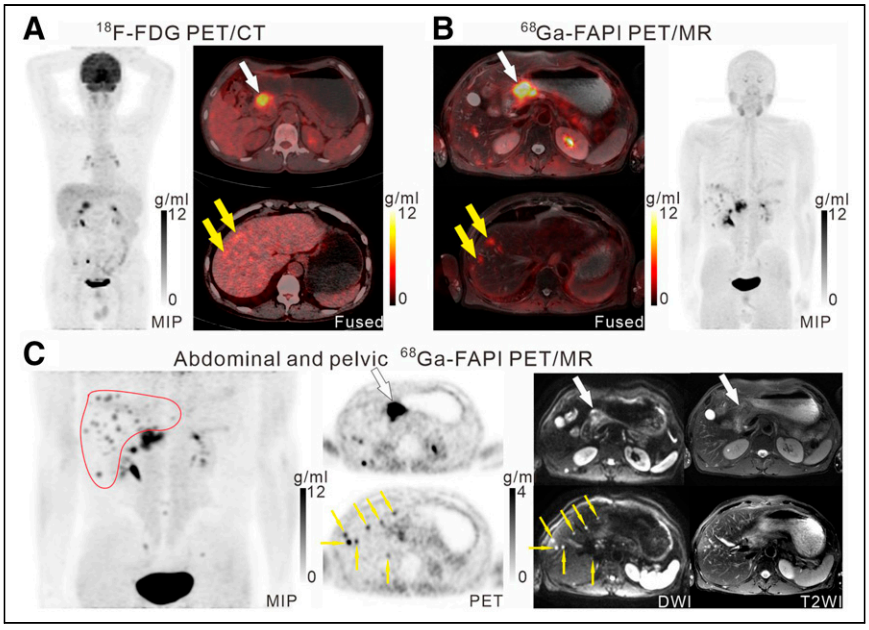

FIGURE 3. A 61-y-old man (patient 7) with moderately differentiated gastric adenocarcinoma. In addition to the primary tumor (A, white arrow, SUV_{max} = 11.0), 2 foci of elevated activity in the liver were noted on the ^{18}F-FDG PET/CT images (A, yellow arrows, SUV_{max} = 5.8). On the ^{68}Ga-FAPI PET/MR images, the primary tumor had more intense uptake (B and C, white arrows, SUV_{max} = 14.2), and the 2 hepatic lesions had more prominent ^{68}Ga-FAPI accumulation (B, yellow arrows, SUV_{max} = 7.6). Additionally, multiple foci of increased ^{68}Ga-FAPI activity were also revealed in the liver (C, red outline, yellow arrows), which corresponded to multiple high signals on DWI (yellow arrows), suggesting multiple hepatic metastases.

in 6 patients for recurrence detection. Patient characteristics are listed in Table 1.

Of the 14 patients for initial staging, 4 patients with earlier imaging stages underwent surgery, 1 underwent omental biopsy, and the remaining 9 received antitumor treatment without surgery due to advanced staging. Notably, for the 4 patients who underwent surgery, pathology confirmed that 3 patients had abdominal lymph nodes metastases, which were completely/partially missed by PET scans. ^{68}Ga-FAPI PET results altered 2 patients' staging (patients 6 and 14) compared with those by ^{18}F-FDG PET/CT. Positive findings revealed by the 2 imaging methods are listed in Supplemental Table 1 (supplemental materials are available at http://jnm.snmjournals.org).

Comparison of Detection Rates

For the patient-based analysis, ^{68}Ga-FAPI PET was superior to ^{18}F-FDG PET in visualizing the primary tumor (100.00% [14/14] vs. 71.43% [10/14]) and peritoneal metastases (100.00% [10/10] vs. 40.00% [4/10]). The 2 imaging modalities were equivalent in exploring metastases in the abdominal lymph nodes (11/11 vs. 10/11), liver (3/3 vs. 3/3), bone (3/3 vs. 3/3), ovarian lesions (7/7 vs. 7/7), and positive supradiaphragmatic lymph nodes (6/7 vs. 6/7) (Table 2).

Comparison of Visual Assessment

In comparison to ^{18}F-FDG PET, ^{68}Ga-FAPI PET provided excellent contrast with low background throughout the body (Fig. 1). Moreover, whether it was the primary tumor or metastasis, the lesion detectability of ^{68}Ga-FAPI PET was superior to that of ^{18}F-FDG PET, and the former received a much higher total score (Fig. 2, 87 vs. 13). In particular, ^{68}Ga-FAPI PET detected significantly more or larger lesions than ^{18}F-FDG PET in the primary tumor (23 vs. 1), metastases in the peritoneum (23 vs. 0), abdominal lymph nodes (18 vs. 1), liver (5 vs. 0) (typical case shown in Fig. 3), and bones (7 vs. 0). Additionally, 4 metastases at uncommon sites in 3 patients (uterus metastasis and rectum involvement in 1 patient [Fig. 4], soft-tissue metastasis in the abdominal wall, and left ureteral metastasis) were revealed. However, for the detection of ovarian lesions (5 vs. 3) (Fig. 5) and positive lymph nodes above the diaphragm (4 vs. 8), ^{68}Ga-FAPI PET had no obvious advantage compared with ^{18}F-FDG.

Comparison of Quantitative Assessment

Table 2 shows metabolic parameters (including original and normalized SUV_{max}) between ^{68}Ga-FAPI and ^{18}F-FDG. Both the original and the normalized SUV_{max} of the primary tumor on ^{68}Ga-FAPI PET were higher than those on ^{18}F-FDG PET. For patient-based analysis, there was no statistically significant difference between original $SUV_{max\text{-}FAPI}$ and $SUV_{max\text{-}FDG}$ of the metastasis with highest activity in each organ/region, and the normalized indicators only affected the results in the abdominal lymph nodes ($P = 0.086$ changed to $P = 0.003$) and hepatic metastases ($P = 0.741$ changed to $P = 0.037$). For lesion-based analysis, the number of lesions in the peritoneum, abdominal lymph nodes, liver, and bone on ^{68}Ga-FAPI PET was greater than that on ^{18}F-FDG PET. Remarkably, the normalized values of $SUV_{max\text{-}FAPI}$ were significantly higher than those of ^{18}F-FDG for all lesions.

Additional Value of MR

Multiple sequences of MR enhanced the interpretation confidence in hepatic metastases in 3 patients (Fig. 3), uterine and rectal metastases in 1 patient (Fig. 4), ovarian lesions in 7 patients (6 metastases [Fig. 5] and 1 corpus luteum as a false-positive finding [Figure 6]), and osseous metastases in 2 patients.

DISCUSSION

In this preliminary study, we found that ^{68}Ga-FAPI PET imaging was superior to ^{18}F-FDG PET imaging in detecting primary lesions and metastases in patients with gastric cancer at the initial diagnosis and recurrence detection, as ^{68}Ga-FAPI PET detected more or larger lesions and showed higher tracer uptake. The low background of ^{68}Ga-FAPI can show small metastatic lesions of gastric cancer in the peritoneum, abdominal lymph nodes, liver, and bone, which are more difficult to detect with ^{18}F-FDG. However, ^{68}Ga-FAPI has physiologic uptake in the uterus and ovaries, which may affect the observation of the corresponding regional lesions. MR has higher soft-tissue contrast and affords multiple sequences, which is conducive to the observation of abdominal and pelvic organs that assists diagnosis. Therefore, ^{68}Ga-FAPI PET/MR exhibited good value in visualizing primary and metastatic gastric cancer.

Previous studies have shown that preoperative ^{18}F-FDG PET/CT has a low detection rate for primary gastric cancer (*14*,*15*). In our study, ^{18}F-FDG PET has a relatively high detection rate of 71.43%

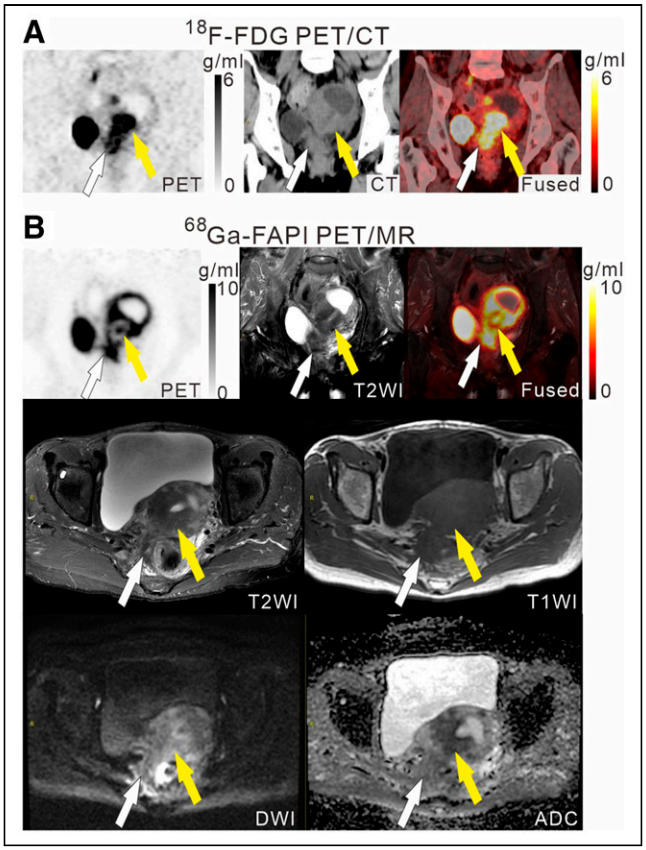

FIGURE 4. A 45-y-old woman (patient 20) with a surgical history of gastric cancer 4 y previously. ^{18}F-FDG PET/CT (A) showed a mass in the uterus with heterogeneous density and intense ^{18}F-FDG activity (yellow arrows, SUV_{max} = 9.1), which involved the adjacent rectum (white arrows, SUV_{max} = 5.7). On ^{68}Ga-FAPI PET/MR (B), there was intense ^{68}Ga-FAPI uptake throughout the uterus (SUV_{max} = 12.7), which may be physiologic uptake. When signal changes on multiple sequences of MR are interpreted, uterine masses (yellow arrows), disappearance of the fat space, and rectal involvement (white arrows) can be observed and diagnosed as metastases. ADC = apparent diffusion coefficient.

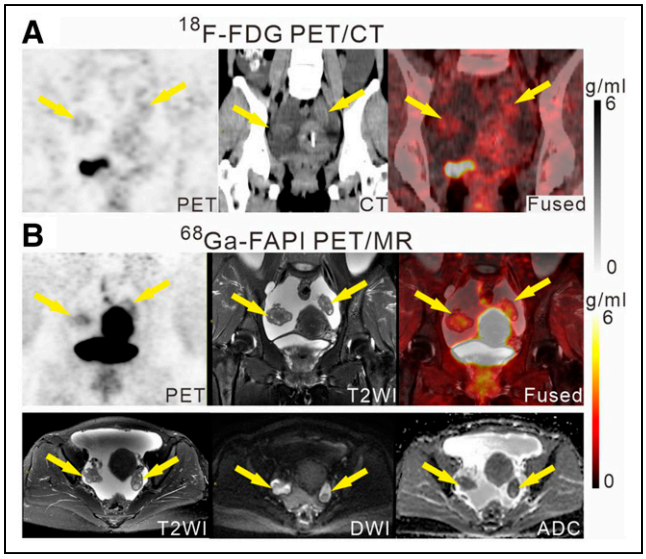

FIGURE 5. Comparison between ^{18}F-FDG PET/CT (A) and ^{68}Ga-FAPI PET/MR (B) for ovarian metastases in a 38-y-old woman (patient 1). Ovaries had slightly increased ^{18}F-FDG accumulation (SUV_{max} = 2.6) (A, arrows); it was difficult to determine whether this accumulation was physiologic uptake or metastases. On ^{68}Ga-FAPI PET/MRI, increased uptake (SUV_{max} = 4.1) was observed in enlarged ovaries with significant MR signal changes (heterogeneous signal on T2-weighted images [T2WI], high signal on DWI, and low signal on apparent diffusion coefficient [ADC]), which enhanced the confidence in making a diagnosis of metastases.

(10/14) for primary tumor detection. This might be because most of these patients were at an advanced stage, with relatively large tumor size/higher malignancy degree. In fact, the uptake of ^{68}Ga-FAPI by the primary tumors was significantly higher than that of ^{18}F-FDG (~2–4×), as shown in our results (Fig. 1). Especially when set against the low background of the gastric area, ^{68}Ga-FAPI–avid lesions will be particularly obvious and easily visualized. A recent comparative study demonstrated much higher sensitivity of ^{68}Ga-FAPI PET/CT than that of ^{18}F-FDG PET/CT in the detection of primary gastric tumors (100.00% [11/11] vs. 36.36% [4/11]), and the former had higher tracer uptake (SUV_{max}: 12.7 vs. 3.7 $P = 0.03$) (*15*). These findings are consistent with our results. Notably, because most patients in this cohort had distant metastases, the evaluation of the degree of invasion and involvement of the primary tumor was of little significance to staging. Therefore, we only compared the involved area of the primary tumor visualized by the 2 imaging modalities; assessment associated with T staging was not performed. In addition, ^{68}Ga-FAPI PET imaging changed only 2 patients' staging (2/14, 14.3%), which is attributed to the staging proportion of patients. Most of the enrolled patients were in stage IV (11/14, 78.5%). Although our results show that ^{68}Ga-FAPI PET can display more lesions than ^{18}F-FDG PET, for patients with multiple distant metastases, however, it does not change the clinical staging or further affect treatment decisions.

Our results showed that although ^{18}F-FDG PET and ^{68}Ga-FAPI PET were equally effective in visualizing and determining whether metastases existed in a given region, in terms of the lesions' number/area, ^{68}Ga-FAPI had significantly better detectability. Because there were too many, even countless metastatic lesions in some regions (such as the peritoneum and the abdominal lymph nodes), establishing a visual scoring system simplified the comparison. Our scoring system intuitively displayed that ^{68}Ga-FAPI PET outperformed ^{18}F-FDG PET in identifying lesions, especially the peritoneal, abdominal lymph node, hepatic, and osseous metastases, which was consistent with the results of previous publications (*11*,*16*). This can be attributed to the higher sensitivity and the lower gastrointestinal background of ^{68}Ga-FAPI. The latter was an important factor limiting ^{18}F-FDG PET, especially because with peristaltic activity, the heterogeneous uptake in the intestinal wall would increase the difficulty of interpretation by ^{18}F-FDG PET/CT (*17*). Although the superiority of ^{68}Ga-FAPI PET in detecting peritoneal metastases did not significantly change the staging of gastric cancer, it can more accurately determine the involvement extent, which can be used for evaluation of the response to treatment.

The usefulness of ^{18}F-FDG PET/CT in gastric cancer with lymph node metastasis also remains controversial (*14*,*18*). We found that ^{68}Ga-FAPI PET was indeed superior to ^{18}F-FDG PET in visualizing abdominal lymph node metastases, which was similar to the conclusions of other studies (*8*,*10*,*11*). Although ^{18}F-FDG PET had higher scores than ^{68}Ga-FAPI PET in detecting

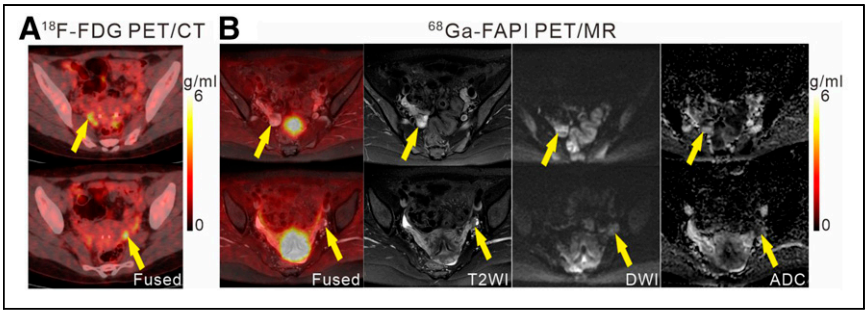

FIGURE 6. Corpus luteum as false-positive on ^{18}F-FDG PET/CT and ^{68}Ga-FAPI PET/MR in a 35-y-old woman (patient 12). Two foci of increased ^{18}F-FDG activity (A, arrows, SUV_{max} = 5.0 [right], 5.7 [left]) and ^{68}Ga-FAPI activity (B, arrows, SUV_{max} = 4.3 [right], 3.3 [left]) were observed in ovaries, but without obvious abnormal morphology and signal changes on MR images (B). Operative exploration confirmed these "lesions" as corpus luteum. ADC = apparent diffusion coefficient.

supradiaphragmatic lymph nodes. However, because of the lack of pathologic proof and the common presence of false-positive on ^{18}F-FDG PET imaging (*19*), whether the ^{18}F-FDG–positive/^{68}Ga-FAPI–negative lesions were truly metastases remained to be determined.

According to our results, both ^{18}F-FDG PET/CT and ^{68}Ga-FAPI PET were ambiguous for the interpretation of ovarian lesions due to the physiologic uptake of ^{18}F-FDG (*20*) or ^{68}Ga-FAPI (Fig. 6) in the ovaries in premenopausal women. MR has been playing an increasing role in the evaluation of gastrointestinal diseases (*21*). Therefore, we introduced PET/MR to explore the additional value of MR, which assisted in the interpretation of some lesions in the ovary, uterus, liver, or bone because of the excellent soft-tissue resolution and more valuable information provided by multiple sequences (*22*).

The present study had several limitations. First, the limited number of patients and pathologic types might cause bias. Second, T staging–related assessments were not conducted because most enrolled patients were in advanced stage. Whether ^{68}Ga-FAPI PET/MR can be beneficial for the staging of patients with gastric cancer in earlier stage needs further assessment. Third, most (9/14) patients did not undergo surgery or biopsy for metastatic lesions. For some patients, although surgery was performed, not all lesions were removed for pathologic examination, especially the supradiaphragmatic lymph nodes. These limiting factors may result in lack of gold standard for the positive lesions. Therefore, we should conduct a clinical trial involving a larger number of gastric cancer patients with comprehensive pathologic types and earlier stage to remedy these limitations and further confirm our results.

CONCLUSION

Compared with ^{18}F-FDG PET/CT, ^{68}Ga-FAPI PET/MR had superior detection capabilities for primary tumors and metastases in the peritoneum, abdominal lymph nodes, liver, and bones in patients with gastric cancer. The detection ability of ^{68}Ga-FAPI PET for ovarian metastases was not better than that of ^{18}F-FDG PET; however, when combined with hybrid MRI ^{68}Ga-FAPI PET/MR could be helpful for avoiding misdiagnosis. In general, ^{68}Ga-FAPI PET/MR outperformed ^{18}F-FDG PET/CT in visualizing primary and metastatic lesions of gastric cancer and may potentially replace ^{18}F-FDG PET/CT.

DISCLOSURE

This study was supported in part by the National Natural Science Foundation of China (no. 81873906 and 81401444). No other potential conflict of interest relevant to this article was reported.

ACKNOWLEDGMENT

We thank Wenyu Song for providing help in drawing part of the graphical abstract.

KEY POINTS

QUESTION: Is ^{68}Ga-FAPI PET/MR superior to ^{18}F-FDG PET/CT in detecting the primary tumor and metastases of gastric cancer?

PERTINENT FINDINGS: In a cohort of 20 patients with gastric cancer, ^{68}Ga-FAPI PET/MR showed a higher detection rate, more lesions, and higher uptake than ^{18}F-FDG PET/CT in both primary lesions and most metastatic organs or tissues.

IMPLICATIONS FOR PATIENT CARE: ^{68}Ga-FAPI PET/MR outperformed ^{18}F-FDG PET/CT in visualizing primary and metastatic lesions of gastric cancer and may potentially replace ^{18}F-FDG PET/CT.

REFERENCES

1. Ferlay J, Soerjomataram I, Dikshit R, et al. Cancer incidence and mortality worldwide: sources, methods and major patterns in GLOBOCAN 2012. *Int J Cancer.* 2015;136:E359–E386.
2. Song Z, Wu Y, Yang J, Yang D, Fang X. Progress in the treatment of advanced gastric cancer. *Tumour Biol.* 2017;39:1010428317714626.
3. Lim JS, Yun MJ, Kim MJ, et al. CT and PET in stomach cancer: preoperative staging and monitoring of response to therapy. *Radiographics.* 2006;26:143–156.
4. Filik M, Kir KM, Aksel B, et al. The role of ^{18}F-FDG PET/CT in the primary staging of gastric cancer. *Mol Imaging Radionucl Ther.* 2015;24:15–20.
5. Kitajima K, Nakajo M, Kaida H, et al. Present and future roles of FDG-PET/CT imaging in the management of gastrointestinal cancer: an update. *Nagoya J Med Sci.* 2017;79:527–543.
6. Stahl A, Ott K, Weber WA, et al. FDG PET imaging of locally advanced gastric carcinomas: correlation with endoscopic and histopathological findings. *Eur J Nucl Med Mol Imaging.* 2003;30:288–295.
7. Hamson EJ, Keane FM, Tholen S, Schilling O, Gorrell MD. Understanding fibroblast activation protein (FAP): substrates, activities, expression and targeting for cancer therapy. *Proteomics Clin Appl.* 2014;8:454–463.
8. Kratochwil C, Flechsig P, Lindner T, et al. ^{68}Ga-FAPI PET/CT: tracer uptake in 28 different kinds of cancer. *J Nucl Med.* 2019;60:801–805.
9. Giesel FL, Kratochwil C, Lindner T, et al. ^{68}Ga-FAPI PET/CT: biodistribution and preliminary dosimetry estimate of 2 DOTA-containing FAP-targeting agents in patients with various cancers. *J Nucl Med.* 2019;60:386–392.
10. Chen H, Pang Y, Wu J, et al. Comparison of [^{68}Ga]Ga-DOTA-FAPI-04 and [^{18}F]FDG PET/CT for the diagnosis of primary and metastatic lesions in patients with various types of cancer. *Eur J Nucl Med Mol Imaging.* 2020;47:1820–1832.
11. Chen H, Zhao L, Ruan D, et al. Usefulness of [^{68}Ga]Ga-DOTA-FAPI-04 PET/CT in patients presenting with inconclusive [^{18}F]FDG PET/CT findings. *Eur J Nucl Med Mol Imaging.* 2021;48:73–86.

12. Fan C, Guo W, Su G, Chen B, Chen H. Widespread metastatic gastric signet-ring cell carcinoma shown by ^{68}Ga-FAPI PET/CT. *Clin Nucl Med.* 2021;46:e78–e79.
13. Pang Y, Huang H, Fu L, Zhao L, Chen H. ^{68}Ga-FAPI PET/CT detects gastric signet-ring cell carcinoma in a patient previously treated for prostate Cancer. *Clin Nucl Med.* 2020;45:632–635.
14. Oh HH, Lee SE, Choi IS, et al. The peak-standardized uptake value (P-SUV) by preoperative positron emission tomography-computed tomography (PET-CT) is a useful indicator of lymph node metastasis in gastric cancer. *J Surg Oncol.* 2011; 104:530–533.
15. Pang Y, Zhao L, Luo Z, et al. Comparison of ^{68}Ga-FAPI and ^{18}F-FDG Uptake in Gastric, Duodenal, and Colorectal Cancers. *Radiology.* 2021;298:393–402.
16. Zheng J, Yao S. [^{68}Ga]Ga-DOTA-FAPI-04 and [^{18}F] FDG PET/CT for the diagnosis of primary and metastatic lesions in patients with hepatic cancer. *Eur J Nucl Med Mol Imaging.* 2020;47:2078–2079.
17. Kitajima K, Murakami K, Sakamoto S, Kaji Y, Sugimura K. Present and future of FDG-PET/CT in ovarian cancer. *Ann Nucl Med.* 2011;25:155–164.
18. Yang QM, Kawamura T, Itoh H, et al. Is PET-CT suitable for predicting lymph node status for gastric cancer? *Hepatogastroenterology.* 2008;55:782–785.
19. Chang JM, Lee HJ, Goo JM, et al. False positive and false negative FDG-PET scans in various thoracic diseases. *Korean J Radiol.* 2006;7:57–69.
20. Nishizawa S, Inubushi M, Okada H. Physiological ^{18}F-FDG uptake in the ovaries and uterus of healthy female volunteers. *Eur J Nucl Med Mol Imaging.* 2005;32: 549–556.
21. Liu B, Ramalho M, AlObaidy M, et al. Gastrointestinal imaging-practical magnetic resonance imaging approach. *World J Radiol.* 2014;6:544–566.
22. Morisawa N, Kido A, Koyama T, et al. Changes of the normal ovary during menstrual cycle in reproductive age on the diffusion-weighted image. *J Comput Assist Tomogr.* 2012;36:319–322.